THE JOURNAL OF BIOLOGICAL CHEMISTRY VOL. 284, NO. 2, pp. 1009–1017, January 9, 2009
© 2009 by The American Society for Biochemistry and Molecular Biology, Inc. Printed in the U.S.A.

# Destruction of Amyloid Fibrils of a $\beta_2$-Microglobulin Fragment by Laser Beam Irradiation*[S]

Received for publication, July 7, 2008, and in revised form, November 3, 2008 Published, JBC Papers in Press, November 14, 2008, DOI 10.1074/jbc.M805118200

**Daisaku Ozawa[‡], Hisashi Yagi[‡], Tadato Ban[§], Atsushi Kameda[‡], Toru Kawakami[‡], Hironobu Naiki[¶], and Yuji Goto[‡1]**

*From the [‡]Institute for Protein Research, Osaka University and CREST, Japan Science and Technology Agency, Yamadaoka 3-2, Suita, Osaka 565-0871, Japan, the [§]National Institute of Advanced Industrial Science and Technology, Midorigaoka 1-8-31, Ikeda, Osaka 563-8577, Japan, and the [¶]Department of Pathological Sciences, Faculty of Medical Sciences, University of Fukui and CREST, Japan Science and Technology Agency, Matsuoka, Fukui 910-1193, Japan*

**To understand the mechanism by which amyloid fibrils form, we have been making real-time observations of the growth of individual fibrils, using total internal fluorescence microscopy combined with an amyloid-specific fluorescence dye, thioflavin T (ThT). At neutral pH, irradiation at 442 nm with a laser beam to excite ThT inhibited the fibril growth of $\beta_2$-microglobulin ($\beta$2-m), a major component of amyloid fibrils deposited in patients with dialysis-related amyloidosis. Examination with a 22-residue K3 fragment of $\beta$2-m showed that the inhibition of fibril growth and moreover the destruction of preformed fibrils were coupled with the excitation of ThT. Several pieces of evidence suggest that the excited ThT transfers energy to ground state molecular oxygen, producing active oxygen, which causes various types of chemical modifications. The results imply a novel strategy for preventing the deposition of amyloid fibrils and for destroying preformed amyloid deposits.**

Amyloid fibrils are associated with the pathogenesis of more than 20 serious diseases, including Alzheimer, Parkinson, and Huntington diseases, and dialysis-related amyloidosis (1, 2). Moreover, various proteins and peptides that are not related to diseases can also form amyloid-like fibrils, implying that the formation of fibrils is a generic property of proteins and peptides (1). In basic structure, amyloid fibrils are long and often twisted, a few nanometers in diameter, and predominantly composed of cross $\beta$-sheets (1, 3). Amyloid fibrils are formed spontaneously with a lag phase or seed-dependently without a lag time, indicating that they are formed by nucleation and extension. Further understanding of the structure, mechanism of formation, and roles in amyloidosis is one of the most important issues of protein science today.

To study amyloid fibrils, we developed a unique technique for their direct observation in which total internal reflection fluorescence microscopy (TIRFM)[2] is combined with amyloid-specific thioflavin T (ThT) fluorescence (4–8). This technique provides important information about the morphology, growth rate, and extension direction of fibrils in real time at the single fibril level. We have applied the technique to the fibrils of $\beta_2$-microglobulin ($\beta$2-m) responsible for dialysis-related amyloidosis and amyloid $\beta$ associated with Alzheimer disease (4–8).

$\beta$2-m is a major component of amyloid fibrils deposited in dialysis-related amyloidosis, a common and serious complication in patients receiving hemodialysis for more than 10 years (9–11). $\beta$2-m, a typical immunoglobulin domain made of 99 amino acid residues and seven $\beta$-stands, is present as the nonpolymorphic light chain of the class I major histocompatibility complex (12). Renal failure disrupts the clearance of $\beta$2-m from the serum and, moreover, $\beta$2-m does not pass through the dialysis membrane, resulting in an increase in the concentration of $\beta$2-m in blood by up to 50-fold. Although an increase in the concentration of $\beta$2-m is the most important risk factor for fibrillation, how $\beta$2-m forms amyloid fibrils under physiological conditions is unknown.

*In vitro* at acidic pH, the incubation of $\beta$2-m in the presence or absence of seed fibrils results in high yields of amyloid fibrils with a range of different morphologies (13–15). However, the generation of $\beta$2-m amyloid fibrils under physiological conditions at neutral pH, where fibrils deposit in patients, has been difficult. Recently, several groups have established conditions under which fibril growth is possible at neutral pH (16–22). For example, Yamamoto *et al.* (16, 17) found that fibrils of $\beta$2-m formed at neutral pH in the presence of trifluoroethanol or SDS. On the other hand, it has been reported that a 22-residue K3 peptide of $\beta$2-m, the sequence $Ser^{20}$-Asn-Phe-Leu-Asn-Cys-Tyr-Val-Ser-Gly-$Phe^{30}$-His-Pro-Ser-Asp-Ile-Glu-Val-Asp-Leu-$Leu^{40}$-$Lys^{41}$ obtained by digestion with *Acromobacter* protease I forms amyloid fibrils spontaneously at neutral pH (23). In addition, it has been reported that K3 peptide forms amyloid fibrils over a wide range of pH and solvent conditions (23–25). Because the K3 peptide is one of the core regions of $\beta$2-m amyloid fibrils

* This work was supported by the Takeda Science Foundation and by Grants-in-Aid from the Japanese Ministry of Education, Culture, Sports, Science and Technology on Priority Areas (No. 40153770). The costs of publication of this article were defrayed in part by the payment of page charges. This article must therefore be hereby marked "*advertisement*" in accordance with 18 U.S.C. Section 1734 solely to indicate this fact.

[S] The on-line version of this article (available at http://www.jbc.org) contains supplemental Fig. S1, Table S1, and Movies S1 and S2.

[1] To whom correspondence should be addressed. E-mail: ygoto@protein.osaka-u.ac.jp.

[2] The abbreviations used are: TIRFM, total internal reflection fluorescence microscopy; $\beta$2-m, $\beta_2$-microglobulin; ThT, thioflavin T; PVS, polyvinylsulfonate; PEI, polyethyleneimine; HPLC, high-pressure liquid chromatography; GdnHCl, guanidine hydrochloride; AFM, atomic force microscopy; PDT, photodynamic therapy.



This is an Open Access article under the CC BY license.

(26), it is thought to play a crucial role in the fibrillation process.

We have started examining the fibrillation process under these neutral pH conditions with TIRFM combined with ThT. We also compare the formation of K3 fibrils with that of whole β2-m fibrils. When we performed real time observations of β2-m and K3 fibrils at neutral pH, fibril extension stopped during TIRFM. Furthermore, preformed K3 fibrils tended to disappear during the observation period. In this report, we focused on clarifying the effects of the laser beam on K3 fibrils. The results showed that the fibrils were decomposed by the irradiation in which ThT molecules bound to fibrils play critical roles. Our results suggest that it may be possible to selectively breakdown amyloid fibrils coupled with amyloid-specific dyes like ThT, suggesting a new strategy for destroying amyloid fibrils ultimately leading to the prevention and treatment of amyloidosis.

## EXPERIMENTAL PROCEDURES

*Materials*—Recombinant human β2-m was expressed with an *Escherichia coli* expression system and purified as described previously (27). A Met residue was always present at the N-terminal position of the recombinant β2-m. In this report, chemically synthesized K3 peptides were purchased from Peptide Institute, Inc. (Osaka, Japan), its purity being >95% according to the elution pattern from reverse phased high-pressure liquid chromatography (HPLC).

*Chemical Modification of Surfaces*—Polyvinylsulfonate (PVS: $M_r$ unknown) was purchased from Sigma. Polyethyleneimine (PEI: $M_r$ 60,000) was obtained from Nacalai tesque (Kyoto, Japan). The surface of quartz slides was modified by adsorbing polyelectrolytes as described before (6). The slides were first cleaned with 0.5% (v/v) Hellmanex (Hellma, Müllheim, Germany)/water and then treated with a solution of acetone for 15 min, rinsed extensively with distilled water, and finally dried in a vacuum oven at 100 °C. Positively charged surfaces were prepared by the adsorption of PEI by incubating quartz in aqueous solutions of PEI (0.1% w/v). Negatively charged surfaces were prepared by layer-by-layer deposition of polyelectrolytes. The former type was created by the adsorption of PVS onto positively charged surfaces of PEI.

*Direct Observation of Amyloid Fibrils*—The TIRFM system used to observe individual amyloid fibrils was developed based on an inverted microscope (IX70, Olympus, Tokyo, Japan) as described (4, 5). The ThT molecule was excited at 442 nm by a helium-cadmium laser (IK5552R-F, Kimmon, Tokyo, Japan). The laser power was 4–80 milliwatt, and the observation period was 3–5 s. The fluorescence image was filtered with a bandpass filter (D490/30, Omega Optical, Bratteboro, VT) and visualized using a digital steel camera (DP70, Olympus).

In the case of β2-m, seeds of β2-m were prepared by fragmentation of amyloid fibrils with a TAITEC (Saitama, Japan) VP-30S sonicator equipped with a microtip. The seeds were added at a final concentration of 30 μg/ml to 25 μM (0.30 mg/ml) β2-m in 50 mM sodium phosphate (pH 7.0) containing 100 mM NaCl and 0.5 mM SDS. ThT solution was then added at a final concentration of 5 μM. In the case of K3, K3 (100 μM, 0.25 mg/ml) was incubated in 50 mM sodium phosphate buffer (pH 6.0) containing 100 mM NaCl. ThT was added at a final concentration of 10 μM. An aliquot (14 μl) of each sample solution was deposited on each microscopic slide, and an image of the fibrils was obtained with TIRFM. The formation of β2-m fibrils and K3 fibrils on various surfaces was also examined. After the mixing of the solutions of seeds, monomeric proteins, and ThT at the same final concentrations as above, the mixture was immediately deposited on the microscopic slide, tightly sealed with a coverslip, and incubated at 37 °C.

*Effect of Laser Beam on Preformed K3 Fibrils*—To examine the effect of laser irradiation, intermittent irradiation on K3 fibrils was performed. The fibrils formed on the PEI/PVS surface were irradiated by a helium-cadmium laser. The irradiation time was 3–5 s, and the laser power was 40–60 milliwatt. It is noted that the laser irradiation points were also the observation points. Then, the relation between laser power and disappearance of fibrils were examined by observing the fibrils at various laser powers. The fibrils were irradiated for 3 s every 15 min. Fluorescence images of amyloid fibrils visualized with TIRFM were quantified to obtain the time course of fibril destruction. For each TIRFM picture, we calculated the average signal intensity of background ($<I_{bkg}>$) and its standard deviation ($\sigma_{bkg}$) from several parts of the picture where fibrils are absent. Then, we counted the number of pixels whose intensity was larger than the threshold value, which was set $<I_{bkg}> + 5\sigma_{bkg}$. The number of pixels containing fibrils was normalized by that at time 0 under the same laser power.

*ThT Assay and Light Scattering*—To make K3 fibrils, K3 (100 μM) was incubated in 50 mM sodium phosphate buffer (pH 6.0) containing 100 mM NaCl in a test tube at 37 °C. The prepared K3 fibrils were diluted 4-fold with 50 mM sodium phosphate buffer (pH 6.0) containing 100 mM NaCl. ThT was added at a final concentration of 10 μM. The sample was introduced into a glass cell with a 10-mm light path, and then irradiated with a helium-cadmium laser at 442 nm or a helium-neon laser (05LHP928, MELLES GRIOT, Albuquerque, NM) at 632.8 nm continuously under agitation. The laser powers were 30–40 milliwatt and 20 milliwatt for the helium-cadmium laser and helium-neon laser, respectively. To examine the participation of oxygen, the above samples were initially purged with nitrogen or oxygen. When the dissolved oxygen of the sample decreased down to 1 mg/l under nitrogen purging or increased more than 30 mg/l under oxygen purging, the samples were started to irradiate with a laser beam under the purging of nitrogen or oxygen. The laser-irradiated K3 fibrils were monitored by fluorescence analysis with ThT and light scattering. For measurements of ThT assay, the wavelengths for excitation and emission were 445 nm and 485 nm, respectively. For measurements of light scattering, the wavelengths were both set at 350 nm. ThT fluorescence and light scattering were measured using a Hitachi F-7000 spectrofluorometer (Tokyo, Japan) at 37 °C.

*Detection of Singlet Oxygen*—To detect singlet oxygen ($^1O_2$), singlet oxygen sensor green reagent (Molecular Probes) was used. The reagent was added at a final concentration of 10 μM to the same samples as described in the procedure of "ThT Assay and Light Scattering." For the measurements of green fluorescence of the sensor reagent, the wavelengths for excitation and emission were 504 nm and 525 nm, respectively.

*Ultracentrifuge Measurements*—Sedimentation velocity of the K3 fibrils after laser irradiation for 48 h was measured using a Beckman-Coulter Optima XL-1 analytical ultracentrifuge (Fullerton, CA) with an An-60 rotor and two-channel charcoal-filled Epon cells. The experiments were performed at 4 °C. The data were analyzed using the software Ultrascan 8.0.

*High Pressure Liquid Chromatography and Mass Analysis*—The laser-irradiated K3 fibrils were lyophilized and then dissolved in 6 M guanidine hydrochloride (GdnHCl). The sample was subjected to reverse-phased HPLC performed on a liquid chromatograph (GILSON, Middleton, WI) equipped with a $5C_4$-AR-300 (4.6 mm × 150 mm; Nacalai tesque, Kyoto, Japan). The sample was eluted with a gradient beginning with solvent A (0.05% trifluoroacetic acid) and an increasing percentage of solvent B (0.05% trifluoroacetic acid/acetonitrile) at a flow rate of 0.5 ml/min. All peaks were collected and lyophilized. Samples dissolved in TA buffer (0.1% trifluoroacetic acid in water/acetonitrile = 2:1) were mixed with a matrix ($\alpha$-cyano-4-hydroxy acid in TA buffer) at a ratio of 1:1, and then 2 $\mu$l was deposited onto a target plate. Matrix-assisted laser desorption ionization-time of flight mass spectrometry (Bruker Daltonics) was used for identification.

*Atomic Force Microscopy (AFM)*—A sample solution was spotted on freshly cleaved mica. After standing for 1 min, the residual solution was blown off with compressed air. AFM images were acquired using a Digital Instruments Nanoscope IIIa scanning microscope at 25 °C (Veeco, Tokyo, Japan). Measurements were performed in an air-tapping mode.

*Amino Acid Analysis*—Amino acid analysis was performed on a Hitachi L-2000 amino acid analyzer after hydrolysis with constant boiling point HCl (Nacalai Tesque, Kyoto, Japan) at 110 °C for 24 h in an evacuated sealed tube. HPLC was carried out on a cation ion exchange column. The amino acids were detected by the reaction with ninhydrin.

## RESULTS

*Effects of Various Surfaces on β2-m and K3 Fibrils*—To observe individual amyloid fibrils with TIRFM, it is necessary to investigate the best conditions for fibril growth. First, β2-m and K3 fibrils were grown in test tubes at pH 7.0 and pH 6.0, respectively, based on the conditions established in our previous studies (23, 28). TIRFM images indicated the presence of short fibrils in each sample (data not shown), confirming that amyloid-specific fluorescence from ThT enables to the visualization of both β2-m and K3 fibrils.

Then, we examined the growth of β2-m and K3 fibrils on the surface of various chemically modified slides. TIRFM images taken after incubation for 12 h often showed radial extensions to both fibrils (Fig. 1). Interestingly, the growth of β2-m fibrils was independent of the properties of the surface (Fig. 1, *A–C*), although that of K3 fibrils varied depending on the surface (Fig. 1, *D–F*). The growth of K3 fibrils on the negatively charged PEI/PVS surface was explosive (Fig. 1*F*), while that on the positively charged PEI surface was less extensive (Fig. 1*E*). The results indicate that the effects of the surface differ depending on the fibrils. It should be noted that both β2-m and K3 are negatively charged at neutral pH: the net charge at pH 7.0 is −3 for β2-m and that at pH 6.0 is −1 for K3 peptide (23). To

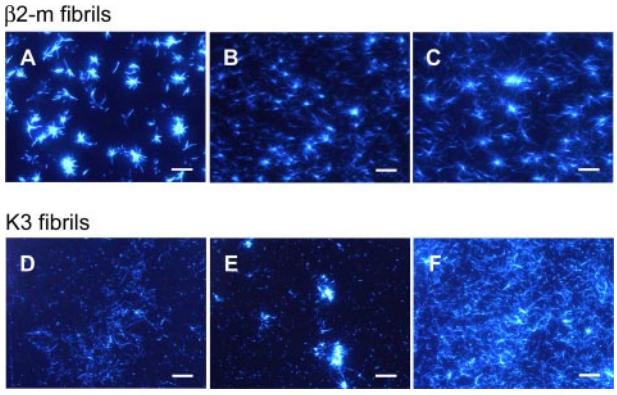


FIGURE 1. **Surface-dependent growth of β2-m and K3 fibrils.** TIRFM images of β2-m fibrils (*A–C*) and K3 fibrils (*D–F*). The growth was performed on various surfaces: quartz (*A* and *D*), positively charged PEI (*B* and *E*), and negatively charged PEI/PVS (*C* and *F*). Concentrations of β2-m monomers, seeds, and ThT were 25 $\mu$M, 30 $\mu$g/ml, and 5 $\mu$M, respectively. In the case of K3 fibrils, concentrations of K3 monomers and ThT were 100 and 10 $\mu$M, respectively. The fibrils were observed after incubation for 12 h. The *scale bar* represents 10 $\mu$m.

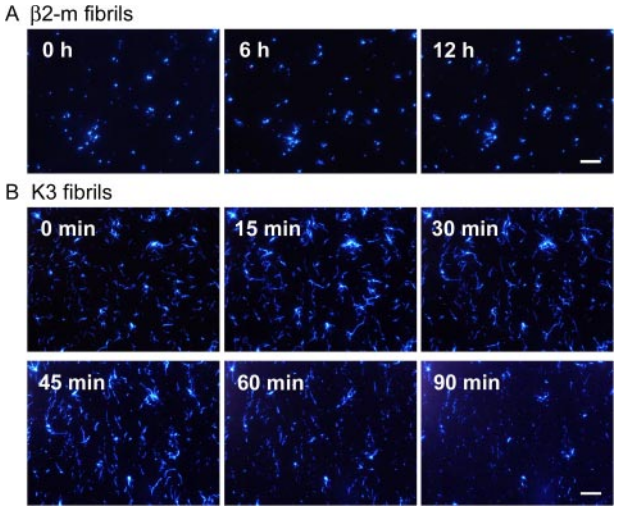


FIGURE 2. **Real-time observations of the growth of β2-m (*A*) and K3 (*B*) fibrils.** β2-m fibrils were extended seed-dependently on the quartz surface and K3 fibrils were extended on the PEI/PVS surface. Concentrations of β2-m monomers, seeds, and ThT were 25 $\mu$M, 30 $\mu$g/ml, and 5 $\mu$M, respectively. As for K3 fibrils, concentrations of K3 monomers and ThT were 100 and 10 $\mu$M, respectively. The extension of β2-m fibrils stopped with time (*A*). In the case of K3, the fibril growth stopped and moreover the fibrils that had formed disappeared (*B*). The *scale bar* represents 10 $\mu$m.

observe the fast growth of these two types of fibrils under optimal conditions, in subsequent experiments, β2-m fibrils were extended seed-dependently on the quartz surface and K3 fibrils, on the PEI/PVS surface.

*Real-time Observations of β2-m and K3 Fibril Growth*—First, we observed the seed-dependent growth of β2-m fibrils at neutral pH (Fig. 2*A*). The laser power was 40–60 milliwatt, and the duration of each irradiation was 3 s. Immediately after the growth was initiated, fluorescent spots of seeds were observed. However, the growth of β2-m fibrils seized during the observation period. Because extensively elongated fibrils were observed in the absence of the laser beam (Fig. 1, *A–C*), we assumed that the growth was inhibited with time by the laser irradiation. In support of this assumption, β2-m fibrils grew normally under a weaker laser power of 4–6 milliwatt (data not shown). There-

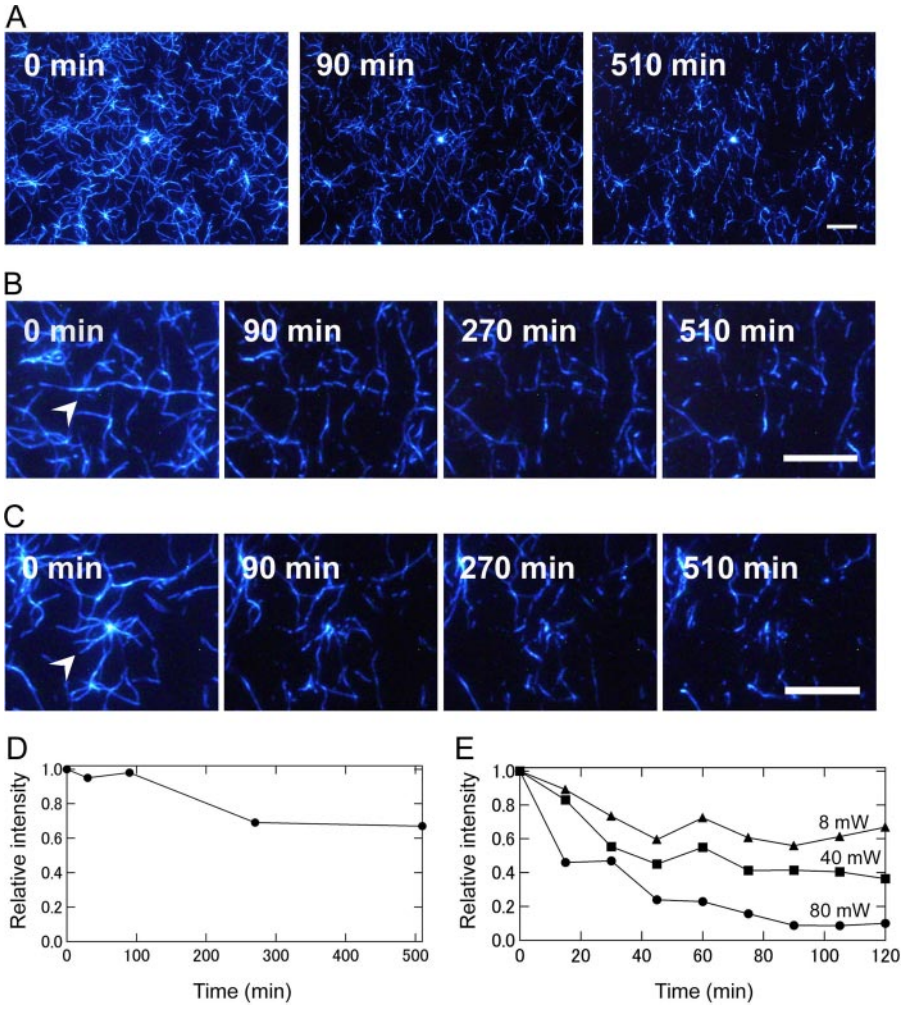


FIGURE 3. **Effects of laser beam on preformed K3 fibrils observed by TIRFM.** *A*, real-time observation of the disappearance of K3 fibrils at pH 6.0 and 37 °C. K3 fibrils were prepared on PEI/PVS in the absence of irradiation under the same conditions as used for the real-time observation of K3 fibril growth. The extended fibrils were then irradiated with a laser beam intermittently at a laser power of 80 mV and a duration of 3–5 s. The scale bar represents 10 $\mu$m. *B* and *C*, interesting images of *A* were expanded and indicated by the *white arrowhead*. *D*, time course of fibril destruction obtained by quantifying TIRFM images shown in *A* (see "Experimental Procedures"). The data points show all of the laser beam irradiation applied. *E*, dependence of fibril destruction on the laser power. The laser power was varied between 8 and 80 milliwatt (*i.e.* 10–100% of *A*) and the duration was 3 s for each irradiation.

fore, the growth of $\beta$2-m fibrils critically depended on the laser beam and its intensity.

Next, real-time observation of the spontaneous fibrillation of K3 was carried out at neutral pH (Fig. 2*B* and supplemental Movie S1). The laser power was 40–60 milliwatt, and the duration was 3 s. At time 0, the fibrils of K3 occurred concomitantly at many sites, implying that the short fibrils had already formed in the sample when K3 peptides were dissolved. Although K3 fibrils extended for a while, producing fibrils as long as several micrometers (see image at 15 min), the growth stopped at 30 min. Moreover, the extended fibrils disappeared with time (images from 45–90 min). However, K3 fibrils also grew under weaker laser irradiation (data not shown). This seizing of fibril growth and moreover the vanishing of preformed fibrils were unexpected events. We assumed that the laser beam caused the inhibition of fibril growth and decomposition of preformed fibrils.

It is noted that the laser beam was applied to the sample for duration of 3 s when we simultaneously obtained TIRFM images. The rest of the time, the sample was incubated in dark. As described below, another possibility is that the apparent fading of fibril images was caused by photobleaching of ThT retaining the fibrils intact. However, no recovery of fibril images during incubation in dark suggests that the disappearance was in fact caused by the destruction of fibrils.

*Disappearance of K3 Fibrils with Irradiation*—To verify the laser-induced inhibition and decomposition, we studied in detail the molecular mechanism involved using K3 peptide, which showed more dramatic effects than the whole $\beta$2-m molecule. In particular, we are interested in the apparent vanishing of K3 fibrils from the TIRFM images.

First, we examined the effect of laser irradiation on preformed K3 fibrils. The fibrils formed on the PEI/PVS surface without any irradiation. Following intermittent irradiation, the fibrils slowly disappeared with time (Fig. 3*A* and supplemental Movie S2). The disappearance occurred locally and discontinuously. These results suggested that K3 fibrils were destroyed by the irradiation coupled with the excitation of ThT. During the laser beam-induced destruction, fibrils vanished concomitantly at various sites in the view (Fig. 3*B*). Meanwhile, radially extended fibrils started to disappear in the vicinity of the growing ends of fibrils (Fig. 3*C*). However, the cores of clustered fibrils resisted destruction. In these single fiber fluorescence images, the diameters of fibrils cannot be determined exactly. The previous study with electron microscopy indicated that K3 fibrils formed under similar conditions at pH 6.5 are made of two types: one with a diameter of ~10 and the other with a diameter of ~5 nm (23). The former are likely to consist of two latter filaments associated laterally.

TIRFM images at various periods were quantified to characterize the time course of the laser beam-dependent fibril disappearance (Fig. 3*D*, see "Experimental Procedures"). The data points represent all of the irradiation events applied, the duration of which was 3–5 s for each. Overall fluorescence intensity estimated for TIRFM image decreased with time (*i.e.* with the number of exposure to the laser beam). Next, to examine the dependence on the laser power, the laser power was varied

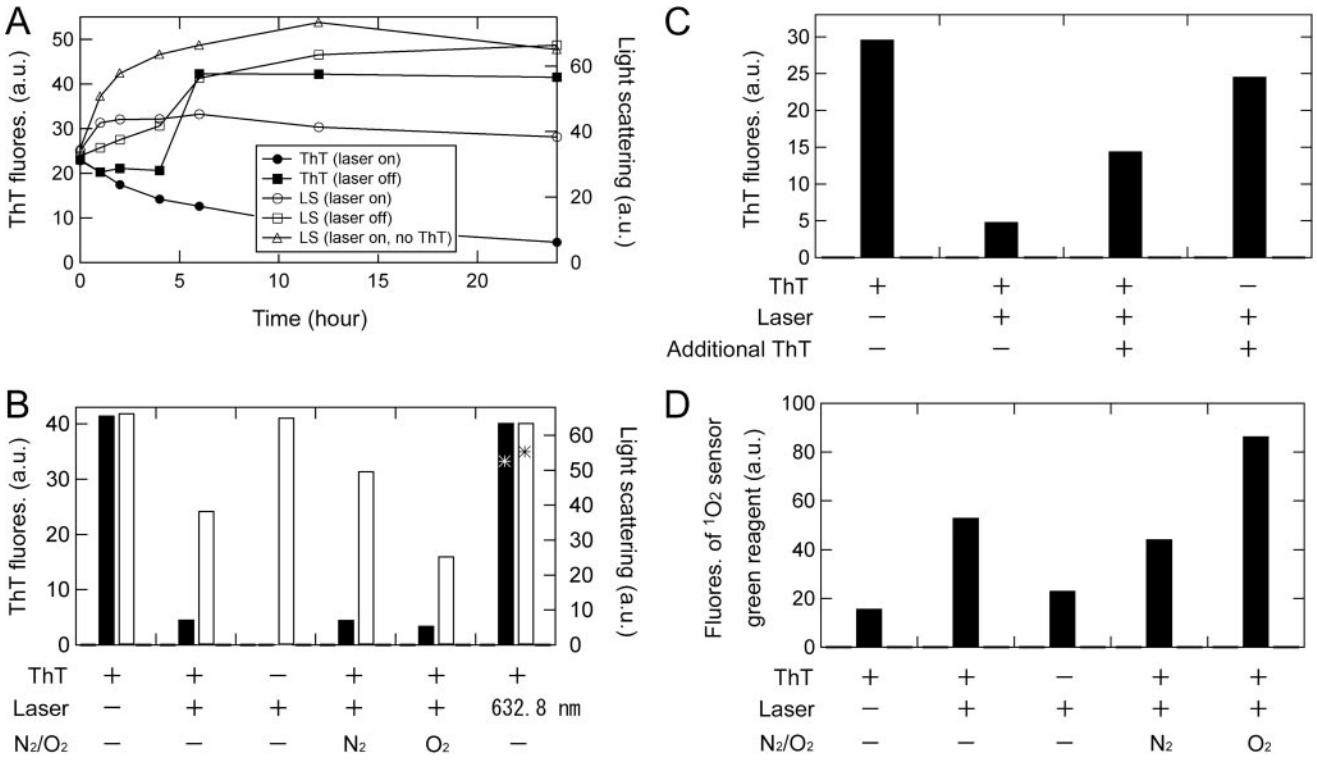


FIGURE 4. **Effects of laser-irradiation on K3 fibrils in bulk solution monitored by ThT fluorescence, light scattering, and singlet oxygen.** *A*, kinetics of the decomposition of K3 fibrils were monitored using ThT fluorescence (●, ■) and light scattering (○, □, △) with (●, ○) or without laser irradiation (■, □), and with laser irradiation in the absence of ThT (△). *B*, the effects of irradiation for 24 h monitored using ThT fluorescence (*left ordinate*, *solid bars*) and light scattering (*right ordinate*, *open bars*) in the presence and absence of ThT, laser irradiation, and nitrogen or oxygen purge. The preformed K3 fibrils were irradiated with a continuous laser beam at 442 nm in the glass cell at pH 6.0 and 37 °C. *632.8 nm* at rightmost indicates that laser irradiation was performed at 632.8 nm by a helium-neon laser. The *asterisks* indicate that the experiments together with the control sample with ThT and without laser-irradiation were performed separately from others, and the values were normalized assuming that the values of the control samples (*leftmost*) are the same. *C*, the effects of additional ThT to irradiated K3 fibrils. Extra ThT at the final concentration 10 $\mu$M was added to the irradiated samples as shown in *B*. *D*, generation of active oxygen upon the excitation of amyloid-bound ThT monitored by singlet oxygen sensor green reagent. In the presence of singlet oxygen, the sensor reagent exhibits green fluorescence at around 525 nm when exited at 504 nm. Conditions were the same as shown in *B*.

between 8 and 80 milliwatt. The duration of laser irradiation was 3 s every 15 min. The destruction was faster and more extensive with an increase in the laser power (Fig. 3*E* and supplemental Fig. S1). These results indicated that the disappearance of K3 fibrils is caused by the laser beam irradiation of ThT bound to fibrils.

*Effects of Laser Irradiation on K3 Fibrils in Bulk Solution*—Although TIRFM images suggested the destruction of K3 fibrils triggered by laser irradiation (Figs. 2 and 3), another possibility is that the apparent fading of images is caused by photobleaching of ThT bound to fibrils. To distinguish between these possibilities, we analyzed the structure of irradiated K3 fibrils in bulk solution. We first prepared K3 fibrils in a test tube. The fibrils were introduced into a glass cell with a 10-mm light path, and then irradiated with a laser beam at 442 nm by a helium-cadmium laser at a power of 30–40 milliwatt continuously under agitation.

As the irradiation proceeded, the intensity of the ThT fluorescence decreased (Fig. 4*A*). Although the intensity of the light scattering increased temporarily, it slightly decreased after about 10 h. Because of the possible fluctuation of the concentration and length of fibrils, it was difficult to reproduce exactly the intensities of light scattering and ThT fluorescence. However, the difference among the different experimental conditions as shown in Fig. 4 was reproducible, indicating that we can address the effects of laser irradiation on the basis of the relative intensities of light scattering and ThT fluorescence. The transient increase of the light scattering is likely attributable to the aggregation of K3 fibrils induced by the stirring because notable increase was observed for the samples without ThT or laser irradiation. After a long period of irradiation, the light scattering intensity was stable as the decrease in ThT intensity ceased. Although the concentration of ThT we used (10 $\mu$M) is close to its CMC (29), the similar light scattering for the sample with ThT and without laser and that without ThT and with laser (Fig. 4, *A* and *B*) suggests that the possible self-aggregation of ThT does not affect the results.

It was thought that the saturation of photobleaching of ThT also stopped the decrease in light scattering intensity. However, the results raise the possibility that the agitation during laser irradiation broke the K3 fibrils. Thus, the same experiment was carried without laser irradiation. The intensity of neither the ThT fluorescence nor light scattering decreased notably, confirming that the effects depend on the irradiation (Fig. 4*A*). Furthermore, when laser excitation at different wavelength (632.8 nm by a helium-neon laser) was used, the results were similar to those without laser irradiation at 442 nm by a helium-cadmium laser (Fig. 4*B*). Then, to examine the participation of ThT, the experiment was carried in the absence of ThT. The light scattering intensity did not decrease (Fig. 4*A*), indicating

that ThT is directly involved in the decrease. In other words, ThT plays a critical role in the laser irradiation-dependent damage of K3 fibrils.

To further investigate the possibility of ThT photobleaching, we added extra ThT (10 $\mu$M) to the irradiated samples after 24 h (Fig. 4*C*). The intensity of ThT fluorescence increased to some extent. However, it was much lower than the level before laser irradiation, confirming that the laser irradiation destructed K3 fibrils. The results also indicated that photobleaching of ThT bound to fibrils partly contribute to the apparent disappearance of ThT fluorescence. As expected, the addition of 10 $\mu$M ThT to the sample irradiated in the absence of ThT brought the high fluorescence value of ThT revealing the minimal damage in the absence of ThT.

We then assumed that active oxygen generated upon the excitation of ThT plays a role (30, 31). To examine the involvement of oxygen in the destruction of K3 fibrils, the samples were purged with nitrogen or oxygen under laser irradiation (Fig. 4*B*). With the nitrogen purged, the intensity of light scattering after 24 h did not decrease significantly. But with the oxygen purged, the intensity decreased at a much greater rate. These results suggested that oxygen is involved in the destruction of K3 fibrils. ThT intensity decreased significantly independent of the purging of nitrogen or oxygen, indicating that substantial fractions of ThT molecules were decomposed by the laser beam, separate from the ThT-coupled decomposition of amyloid fibrils. It is likely that specific binding of ThT to amyloid fibrils accelerates the decomposition of ThT itself: amyloid fibrils catalyze the laser-dependent decomposition of ThT, consuming bulk ThT molecules.

To examine the generation of active oxygen upon the excitation of amyloid bound ThT, we used a singlet oxygen ($^1O_2$) detection reagent (Fig. 4*D*). In the presence of singlet oxygen, the sensor reagent exhibits green fluorescence at around 525 nm when exited at 504 nm. The laser-irradiated sample in the presence of ThT showed high fluorescence. Both ThT and fibrils were required for the high fluorescence. Moreover the fluorescence intensity increased with oxygen purged, whereas it was slightly suppressed with nitrogen purged. These results indicated that singlet oxygen is generated specifically by the laser irradiation of amyloid-bound ThT.

*Analysis of Morphology and Chemical Structure of Laser-irradiated K3 Fibrils*—We also examined the effects of laser irradiation on the morphology of K3 fibrils monitored by AFM. The AFM images revealed the fibrils to be relatively long before the irradiation (Fig. 5*A*) and shortened after the irradiation for 48 h (Fig. 5*B*). To clarify the size distribution of the irradiated K3 fibrils, we performed an analysis of sedimentation velocity. The sedimentation coefficient exhibited several peaks, indicating the existence of various fibrils with different molecular weights (Fig. 5, *C* and *D*). At 226,000 × *g*, the peaks at about 0.5 S and 0.8 S correspond to the K3 monomer (2,498 Da) and dimer, respectively (Fig. 5*D*). It is noted that the K3 peptide has a free thiol at $Cys^{25}$, and the disulfide-linked dimer was produced during the experiments (23). On the other hand, because of the supramolecular structure, non-irradiated K3 fibrils readily precipitated even at 900 × *g*, and we could not analyze their sedimentation velocity (data not shown). These results

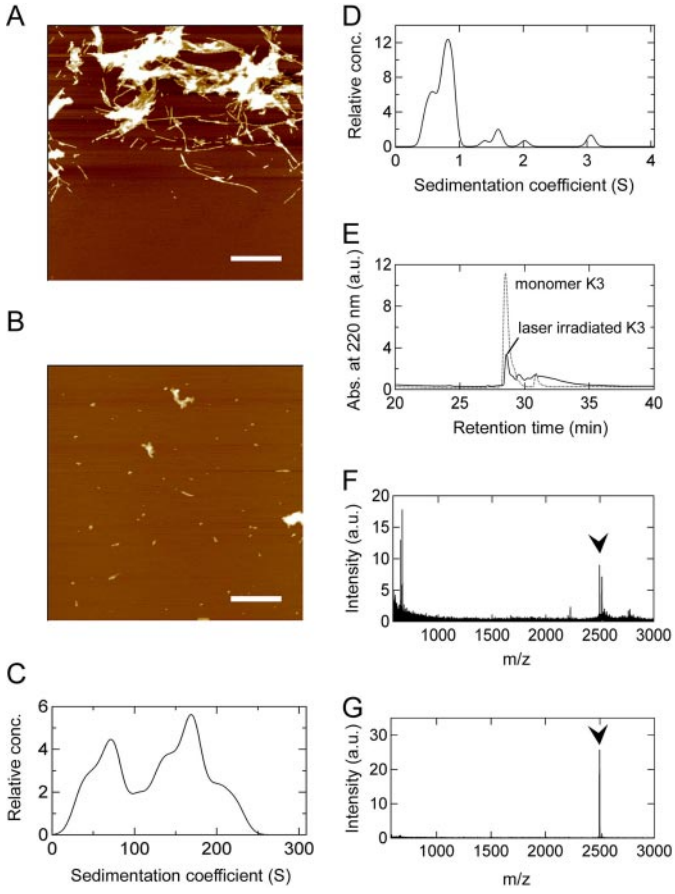


FIGURE 5. **Effects of laser beam irradiation on K3 fibrils monitored by morphology and chemical structure.** *A* and *B*, AFM images of K3 fibrils before (*A*) and after (*B*) laser irradiation. After laser irradiation, only short fibrils and aggregates were observed. The *scale bar* represents 1 $\mu$m. *C* and *D*, the distribution of sedimentation coefficients obtained from the sedimentation velocity measurements of K3 fibrils after laser irradiation. The distribution ranged from 0 to 300 S (*C*) and from 0 to 4 S (*D*). The centrifugation experiments were performed at 5,000 × *g* (*C*) and 226,000 × *g* (*D*), respectively. *E*, elution profile of the K3 monomer (*dotted line*) and laser-irradiated K3 fibrils (*solid line*) monitored by reversed-phase HPLC. K3 fibrils dissolved in 6 M GdnHCl were injected. *F* and *G*, mass spectra of K3 fibrils with (*F*) and without laser irradiation (*G*). The position of intact K3 is indicated by the *arrowhead*. For all of *A*–*G*, the irradiation period was 0 or 48 h.

also confirmed that K3 fibrils were broken down or decomposed by the laser irradiation into shorter fibrils. Moreover, products similar in molecular weight to the K3 monomer existed in the sample of the irradiated fibrils, suggesting that the irradiation brought about chemical modifications damaging the ability of K3 peptides to polymerize.

Then, to investigate whether laser-irradiation causes chemical modifications of K3 fibrils, we carried out analyses using HPLC (Fig. 5*E*) and mass spectroscopy (Fig. 5, *F* and *G*). To analyze the chemical damage to the monomer, irradiated K3 fibrils were dissolved in 6 M GdnHCl. In the HPLC analysis, the sample of dissolved fibrils showed multiple broad peaks (Fig. 5*E*). The peaks with retention times of 28 min and 31 min are those of the K3 monomer and dimer, respectively. As described above, the disulfide-linked dimer was produced during the experiments. When compared with the elution profile of the equivalent amount of fresh K3 solution, the monomeric peak of GdnHCl-treated K3 fibrils was significantly decreased in intensity, instead producing a broad tailing peak. These results indi-

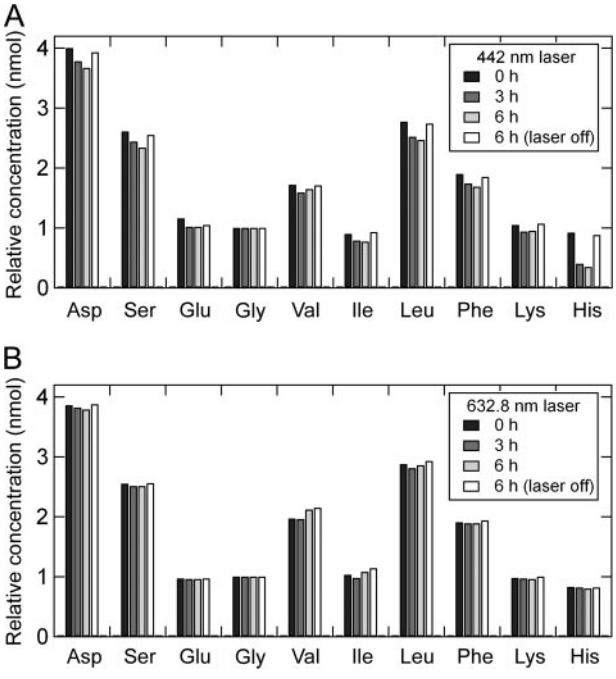


FIGURE 6. **Amino acid analysis of K3 fibrils before and after laser irradiation.** The laser beam irradiations were performed at 442 nm (*A*) and 632.8 nm (*B*) under the same conditions as shown in Fig. 4*A*.

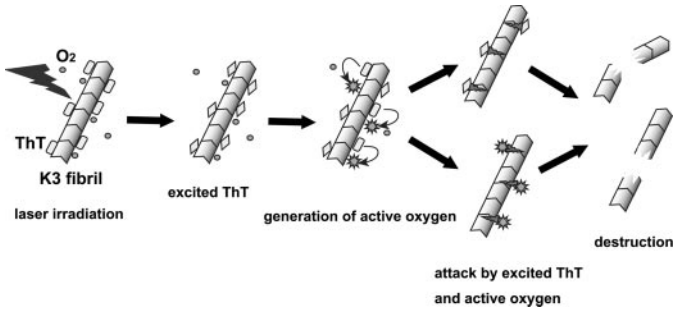


FIGURE 7. **Schematic model of the break up of K3 fibrils by the laser beam.** ThT binds specifically to K3 fibrils, and its optical properties change. Irradiation at 442 nm excites ThT from a ground state. Then, the excited ThT transfers its energy to ground-state molecular oxygen (triplet oxygen), producing singlet oxygen. Labile singlet oxygen attacks directly Tyr, Cys, and His side chains in K3 fibrils. Additionally, excited triplet oxygen generates hydrogen peroxide ($H_2O_2$) and various types of free radicals causing chemical modifications. It is also possible that excited ThT directly attacks K3 fibrils. These lead to the destruction of K3 fibril.

cated the existence of products of various molecular weights, other than the K3 monomer and dimer. Moreover, in comparison with K3 fibrils without irradiation (Fig. 5*G*), the mass analysis of irradiated K3 fibrils revealed several decomposed peaks (*e.g.* $m/z$ = 665 and 2,225) as well as a peak of the monomer ($m/z$ = 2,496) (Fig. 5*F*). Interestingly, these peaks also had a smaller molecular weight than the monomer, suggesting the cleavage of peptide bonds by the laser.

To address the chemical modification further, we performed amino acid analysis (Fig. 6, *A* and *B*). K3 peptide of 22 amino acid residues contains 2 Asp, 2 Asn, 3 Ser, 1 Glu, 1 Pro, 1 Gly, 1 Cys, 2 Val, 1 Ile, 3 Leu, 1 Tyr, 2 Phe, 1 Lys, and 1 His residues. It is known that Tyr, Met, Cys, Trp, and His are amenable to oxidation (30, 31). In this experiment, the contents of Pro, Cys, and Tyr residues were not quantitatively determined. Consistent with these, notable decrease upon laser irradiation was observed for His: after 3 h of irradiation, the intensity decreased to 40% of the reference sample without irradiation (Fig. 6*A* and supplemental Table S1). Other residues shown in Fig. 6*A* exhibited the expected number on the basis of amino acid composition and remained constant during laser-irradiation of 6 h. The results suggest that other amenable residues (*i.e.* Tyr and His) were also modified by active oxygen. In contrast, when laser excitation at 632.8 nm was used, the content of His residue did not decrease confirming that the irradiation of ThT is essential for the laser-induced destruction (Fig. 6*B*).

Taken together, we conclude that K3 fibrils were severely damaged by the irradiation and consequently the fibrils were broken down into shorter fibrils, oligomers and monomers. Furthermore, it is likely that the laser-irradiated K3 fibrils underwent the cleavage of peptide bonds and various chemical modifications.

## DISCUSSION

*Mechanism of the Light-induced Damage of K3 Fibrils*—In this report, we showed that the growth of K3 and $\beta$2-m fibrils is inhibited by irradiation with a laser beam at 442 nm. Furthermore, preformed K3 fibrils were broken down into shorter fibrils and monomers and underwent chemical modifications. The reactions require ThT, indicating that the laser beam-excited ThT plays critical roles. The effects of purging samples with nitrogen or oxygen suggested the participation of active oxygen, in particular, singlet oxygen and oxygen radicals. We confirmed that singlet oxygen is generated by the laser irradiation of amyloid bound ThT. Thus, the excited energy of ThT is transferred to ground-state oxygen (triplet oxygen), producing singlet oxygen and moreover oxygen peroxide and oxygen radicals. These lead to an inhibition of growth and ultimately the destruction of K3 fibrils.

Although the exact mechanism involved is still unclear, we suggest a basic model for the laser beam-dependent decomposition of amyloid fibrils (Fig. 7). First, as described below, ThT binds specifically to K3 fibrils, its optical properties changing as a result (32). The amyloid-bound ThT exhibits strong fluorescence at around 485 nm when excited at 442 nm by a helium-cadmium laser. Upon excitation, ThT transforms from a ground state to an excited state. One possibility is that the excited ThT transfers energy to ground-state molecular oxygen (*i.e.* triplet oxygen), producing singlet oxygen. Another possibility is that excited triplet oxygen generates hydrogen peroxide ($H_2O_2$) and various types of free radicals (31). The active and labile oxygen (*i.e.* singlet oxygen, hydrogen peroxide and oxygen radicals) thus produced attacks nearby amyloid fibrils causing various types of chemical modifications. By performing amino acid analysis, we found that the peak of His decreased significantly. It is likely that Tyr and Cys residues were also damaged (31). Additionally, excited ThT may directly attack K3 fibrils. These events bring about the destruction of fibrils, ultimately producing various chemically modified K3 monomers and shorter peptides.

We consider the mechanism of damage to K3 fibrils to be similar to that caused by photodynamic therapy (PDT). PDT, a promising treatment for cancer, involves the use of photo-

chemical reactions mediated through the interaction of light with photosensitizing agents (33, 34). Through photochemical reactions, various types of active oxygen including singlet oxygen, hydrogen peroxide, and free radicals are generated causing cell death. PDT can select a photo-oxidized target, including deoxyribonucleic acid or protein, depending on the photosensitizing agent, which binds a specific target. Similarly, we showed that ThT, which specifically binds to amyloid fibrils, causes the inhibition of fibril growth and moreover the destruction of fibrils.

Although the reaction takes advantage of the amyloid-specific fluorescence dye ThT, the underlying mechanism of the binding of ThT to amyloid fibrils and consequent dramatic change in fluorescence quantum yield remains unclear (35–38). ThT is made of benzothiazole and aminobenzene rings connected by a rotating single bond, and in the ground state, has a nonplanar conformation. It has been suggested that an excimer formation in cavities which can accommodate two ThT ions is responsible for the characteristic fluorescence (37, 38). On the other hand, a quantum-chemical calculation suggests that, when internal rotation of the dye molecule is blocked because of steric hindrance upon binding to amyloid fibrils, the internal charge-transfer process in the excited singlet state leading to quenching is suppressed, thus producing a high quantum yield of fluorescence (35). Another quantum-chemical calculation suggests that, in the planer excited state, a population of fluorescent ThT molecules with $\pi$-conjugated bonds of benzothiazole and aminobenzene rings is produced (36). To achieve the efficient decomposition of fibrils by laser irradiation, understanding the mode of binding of ThT to fibrils is important.

The difference in the effects of laser irradiation on $\beta$2-m and K3 fibrils may be caused by the difference in the stability and morphology of fibrils. $\beta$2-m fibrils are made of several protofilaments tightly associated laterally, while K3 fibrils represent a single protofilament or the bundles of a couple of protofilaments, which may be different from that of mature $\beta$2-m fibrils (23). $\beta$2-m fibrils were more stable than K3 fibrils against depolymerization induced by pH change (26) or unfolding induced by GdnHCl.[3] In accordance with these observations, $\beta$2-m fibrils were more stable against the laser beam than K3 fibrils. Although the inhibition of fibril growth and decomposition of preformed fibrils were observed for K3 fibrils, only the former was observed for $\beta$2-m fibrils. The rigid architecture of mature $\beta$2-m fibrils may prevent decomposition by the laser, suggesting that the effects directly depend on the stability and rigidity of fibrils.

In contrast, the promoting effects of oxidative stress on fibrillation have been implicated in Alzheimer disease and Parkinson disease (39). Lipid peroxidation products formed via lipid alkoxyl radicals accelerated the fibrillation of amyloid $\beta$ and $\alpha$-synuclein. Thus, although oxidative stress can trigger the formation of fibrils under certain conditions, fine tuning of their effects (*e.g.* extensive photooxidation more than inducing fibril growth) may enable the specific destruction of amyloid fibrils. In fact, we observed the destruction of ThT-bound amyloid $\beta$ fibrils triggered by an extensive laser beam irradiation of ThT,[3] suggesting the generality of the approach reported here. Interestingly, acceleration of fibrillation of amyloid $\beta$ in the presence of ThT by a relatively weak laser irradiation was also observed.[3] The detailed analysis of the adverse effects depending on the laser power is underway and will be published elsewhere.

*Effects of Surfaces on β2-m and K3 Fibril Growth*—Finally, we address the effects of various surfaces on fibril growth because we employed special conditions accelerating the fibril growth. The effects of the surface differed between $\beta$2-m and K3 (Fig. 1). We did not observe a clear dependence of $\beta$2-m fibril formation on the charge of the surface (Fig. 1, *B* and *C*). This independence may be caused by our special conditions including 0.5 mM SDS. On the other hand, K3 fibrils did not grow well on the positively charged PEI surface (Fig. 1*E*), but exhibited explosive growth on the negatively charged PEI/PVS surface (Fig. 1*F*).

Previously, we reported that negatively charged slides enhance the fibril growth of negatively charged amyloid $\beta$-(1–40) and positively charged slides inhibit it (6). Zhu *et al.* (40) similarly reported that amyloidogenic immunoglobulin light chain variable domain SMA with a negative net charge formed fibrils on a negatively charged mica surface, but not on positively charged or hydrophobic surfaces. In this context, it has been reported that collagen plays a crucial role in the deposition of $\beta$2-m amyloid under physiological conditions (20). The authors proposed that positively charged surfaces along the collagen fiber directly enhance the fibrillation of negatively charged $\beta$2-m.

Although electrostatic interaction is important to the formation of $\beta$2-m fibrils, other interactions may also be involved. The net charge of the $\beta$2-m monomer and K3 peptide is $-3$ at pH 7.0 and $-1$ at pH 6.0, respectively. The molecular weights are 11,854 and 2,498, respectively. Thus, it is likely that the fibril growth of K3 is more affected by electrostatic interactions than that of $\beta$2-m.

## CONCLUSION

In conclusion, we revealed that K3 fibrils were decomposed by the laser beam in the presence of amyloid-bound ThT molecules. Although we only observed inhibition of fibril growth for $\beta$2-m, it is likely that ThT-induced decomposition of $\beta$2-m fibrils occurs under appropriate conditions. Because amyloid fibrils have a unique supramolecular structure, it may be possible to create very specific and powerful PDT reagents for them. The present results suggest the light-induced decomposition of amyloid fibrils coupled with an amyloid-specific dye to be useful in the treatment or prevention of dialysis-related amyloidosis, for which no effective method has yet been established.

*Acknowledgments—We thank Miyo Sakai (Institute for Protein Research) for performing ultracentrifuge analysis and Dr. Tetsuichi Wazawa (Tohoku University) for support with the TIRFM system.*

[3] Y. Goto, unpublished results.

## REFERENCES

1. Dobson, C. M. (2003) *Nature* **426,** 884–890
2. Cohen, F. E., and Kelly, J. W. (2003) *Nature* **426,** 905–909

3. Uversky, V. N., and Fink, A. L. (2004) *Biochim. Biophys. Acta* **1698,** 131–153
4. Ban, T., Hamada, D., Hasegawa, K., Naiki, H., and Goto, Y. (2003) *J. Biol. Chem.* **278,** 16462–16465
5. Ban, T., Hoshino, M., Takahashi, S., Hamada, D., Hasegawa, K., Naiki, H., and Goto, Y. (2004) *J. Mol. Biol.* **344,** 757–767
6. Ban, T., Morigaki, K., Yagi, H., Kawasaki, T., Kobayashi, A., Yuba, S., Naiki, H., and Goto, Y. (2006) *J. Biol. Chem.* **281,** 33677–33683
7. Ban, T., Yamaguchi, K., and Goto, Y. (2006) *Acc. Chem. Res.* **39,** 663–670
8. Yagi, H., Ban, T., Morigaki, K., Naiki, H., and Goto, Y. (2007) *Biochemistry* **46,** 15009–15017
9. Gejyo, F., Yamada, T., Odani, S., Nakagawa, Y., Arakawa, M., Kunitomo, T., Kataoka, H., Suzuki, M., Hirasawa, Y., Shirahama, T., Cohen, A. S., and Schmid, K. (1985) *Biochem. Biophys. Res. Commun.* **129,** 701–706
10. Floege, J., and Ketteler, M. (2001) *Kidney Int. Suppl.* **78,** S164–171
11. Yamamoto, S., and Gejyo, F. (2005) *Biochim. Biophys. Acta* **1753,** 4–10
12. Bjorkman, P. J., Saper, M. A., Samraoui, B., Bennett, W. S., Strominger, J. L., and Wiley, D. C. (1987) *Nature* **329,** 506–512
13. Kad, N. M., Thomson, N. H., Smith, D. P., Smith, D. A., and Radford, S. E. (2001) *J. Mol. Biol.* **313,** 559–571
14. Hoshino, M., Katou, H., Hagihara, Y., Hasegawa, K., Naiki, H., and Goto, Y. (2002) *Nat. Struct. Biol.* **9,** 332–336
15. Ivanova, M. I., Sawaya, M. R., Gingery, M., Attinger, A., and Eisenberg, D. (2004) *Proc. Natl. Acad. Sci. U. S. A* **101,** 10584–10589
16. Yamamoto, S., Yamaguchi, I., Hasegawa, K., Tsutsumi, S., Goto, Y., Gejyo, F., and Naiki, H. (2004) *J. Am. Soc. Nephrol.* **15,** 126–133
17. Yamamoto, S., Hasegawa, K., Yamaguchi, I., Tsutsumi, S., Kardos, J., Goto, Y., Gejyo, F., and Naiki, H. (2004) *Biochemistry* **43,** 11075–11082
18. Kihara, M., Chatani, E., Sakai, M., Hasegawa, K., Naiki, H., and Goto, Y. (2005) *J. Biol. Chem.* **280,** 12012–12018
19. Jahn, T. R., Parker, M. J., Homans, S. W., and Radford, S. E. (2006) *Nat. Struct. Mol. Biol.* **13,** 195–201
20. Relini, A., Canale, C., De Stefano, S., Rolandi, R., Giorgetti, S., Stoppini, M., Rossi, A., Fogolari, F., Corazza, A., Esposito, G., Gliozzi, A., and Bellotti, V. (2006) *J. Biol. Chem.* **281,** 16521–16529
21. Calabrese, M. F., and Miranker, A. D. (2007) *J. Mol. Biol.* **367,** 1–7
22. Sasahara, K., Yagi, H., Sakai, M., Naiki, H., and Goto, Y. (2008) *Biochemistry* **47,** 2650–2660
23. Ohhashi, Y., Hasegawa, K., Naiki, H., and Goto, Y. (2004) *J. Biol. Chem.* **279,** 10814–10821
24. Iwata, K., Fujiwara, T., Matsuki, Y., Akutsu, H., Takahashi, S., Naiki, H., and Goto, Y. (2006) *Proc. Natl. Acad. Sci. U. S. A* **103,** 18119–18124
25. Yamaguchi, K., Takahashi, S., Kawai, T., Naiki, H., and Goto, Y. (2005) *J. Mol. Biol.* **352,** 952–960
26. Kozhukh, G. V., Hagihara, Y., Kawakami, T., Hasegawa, K., Naiki, H., and Goto, Y. (2002) *J. Biol. Chem.* **277,** 1310–1315
27. Chiba, T., Hagihara, Y., Higurashi, T., Hasegawa, K., Naiki, H., and Goto, Y. (2003) *J. Biol. Chem.* **278,** 47016–47024
28. Yamamoto, K., Yagi, H., Ozawa, D., Sasahara, K., Naiki, H., and Goto, Y. (2008) *J. Mol. Biol.* **376,** 258–268
29. Khurana, R., Coleman, C., Ionescu-Zanetti, C., Carter, S. A., Krishna, V., Grover, R. K., Roy, R., and Singh, S. (2005) *J. Struct. Biol.* **151,** 229–238
30. Agon, V. V., Bubb, W. A., Wright, A., Hawkins, C. L., and Davies, M. J. (2006) *Free Radic. Biol. Med.* **40,** 698–710
31. Davies, M. J. (2004) *Photochem. Photobiol. Sci.* **3,** 17–25
32. Naiki, H., Higuchi, K., Hosokawa, M., and Takeda, T. (1989) *Anal. Chem.* **177,** 244–249
33. Giuliano, E. A., Ota, J., and Tucker, S. A. (2007) *Vet. Ophthalmol.* **10,** 337–343
34. Buytaert, E., Dewaele, M., and Agostinis, P. (2007) *Biochim. Biophys. Acta* **1776,** 86–107
35. Stsiapura, V. I., Maskevich, A. A., Kuzmitsky, V. A., Turoverov, K. K., and Kuznetsova, I. M. (2007) *J. Phys. Chem. A.* **111,** 4829–4835
36. Maskevich, A. A., Stsiapura, V. I., Kuzmitsky, V. A., Kuznetsova, I. M., Povarova, O. I., Uversky, V. N., and Turoverov, K. K. (2007) *J. Proteome Res.* **6,** 1392–1401
37. Groenning, M., Norrman, M., Flink, J. M., van de Weert, M., Bukrinsky, J. T., Schluckebier, G., and Frokjaer, S. (2007) *J. Struct. Biol.* **159,** 483–497
38. Groenning, M., Olsen, L., van de Weert, M., Flink, J. M., Frokjaer, S., and Jorgensen, F. S. (2007) *J. Struct. Biol.* **158,** 358–369
39. Bieschke, J., Zhang, Q., Bosco, D. A., Lerner, R. A., Powers, E. T., Wentworth, P., Jr., and Kelly, J. W. (2006) *Acc. Chem. Res.* **39,** 611–619
40. Zhu, M., Souillac, P. O., Ionescu-Zanetti, C., Carter, S. A., and Fink, A. L. (2002) *J. Biol. Chem.* **277,** 50914–50922